


# An Improved Method for Determining the Pressure on the Surface of Backfill Bridges

Anatoly Sergeevich Permikin<sup>1,2</sup> <sup>a</sup>, Konstantin Yurievich Astankov<sup>1,2</sup>, Ilya Alexandrovich Osokin<sup>1</sup>,  
Nikita Vyacheslavovich Volkov<sup>2</sup> and Igor Georgievich Ovchinnikov<sup>1</sup>  
<sup>1</sup>Ural State University of Railway Transport, Yekaterinburg, Russia  
<sup>2</sup>Mascot LLC, Yekaterinburg, Russia

**Keywords:** The backfill bridge, the Boussinesq problem, distribution of stresses in the ground, determination of displacements, the theory of a linearly deformable half-space.

**Abstract:** The article discusses the application of the solution of the Boussinesq problem to determine the pressure on the load-bearing arched structure element of a soil-filled bridge structure, taking into account: the distribution of pressure in the soil from the test static load along the widths of the roof of the bearing element, the horizontal component of the pressure from the impact of the static test load, the repulsion of the soil mass due to the introduction bed rest. As a result, the values obtained in the study of the displacements of sections of the bearing element at characteristic points with the values obtained during field tests of a road bridge in the Vologda Region at 156 km of the A—114 Vologda - Novaya Ladoga highway.

## 1 INTRODUCTION

Currently, the spread of backfill bridges is limited due to many factors, one of which is the lack of a simple and logically reflecting the work of the design of the methodology for taking into account temporary loads (Heger, 1982; Heger, 1985).

Such artificial structures are calculated using finite element models created in modern automated software systems (Rubin, 2016; Shamshina, 2018; Permikin, 2020). However, the results obtained with such calculations are difficult to analyze and verify, and the values of the forces in the structural elements are often overestimated (Safronov, 2010). The models themselves are difficult to construct and perceive, and modeling of soil backfill with a lack of experience in designing soil-filling structures is difficult to implement due to the unpredictable behavior of the soil mass over time (Kevin, 2016; Erdogmus, 2010).


In the course of previous research on the topic of an analytical approach to modeling the distribution of pressure from a temporary load (Volkov, 2019), it was noted that the application of the solution of the Boussinesq problem (Khan, 1988; Gorbunov-Posadov, 1985) to determine the pressure on the load-bearing structural element gives unsatisfactory errors

based on the results of comparing the deflections obtained with the deflections obtained during static load tests of the bridge.

The authors propose to improve the laws of pressure distribution and achieve greater convergence of the calculation results with the results of full-scale static tests by introducing the following calculation provisions:

1. accounting for the distribution of pressure in the soil thickness from the static test load along the width of the arch of the bearing element;
2. taking into account the horizontal component of the pressure from the impact of a static test load;
3. taking into account the resistance of the soil massif by introducing the coefficient of subgrade reaction.

To confirm the consistency of the method proposed by the authors for collecting temporary loads on the bearing element of a backfill bridge, a correlation was carried out between the values obtained during the study of the displacement of the sections of the bearing element at characteristic points with the values obtained during field tests of a road bridge in the Vologda Region at 156 km of the A—114 Vologda - Novaya Ladoga highway (Safronov, 2010).

<sup>a</sup> <https://orcid.org/0000-0002-6162-156X>

## 2 INITIAL DATA

The physical and mechanical properties of the soil massif were adopted based on the results of laboratory studies and field tests that have been preserved since the construction (Table 1).

Table 1: The physical and mechanical properties of the soil massif

Modulus of deformation $E$ , MPa	Poisson's ratio $\nu$	Coefficient of adhesion $c$ , MPa	Internal friction angle $\varphi$ , degrees	Ultimate tensile stress $R_t$ , MPa
22.6	0.3	0.001	30	0

To obtain the displacements of the arch nodes in characteristic sections, the authors propose to use the PC "LIRA-CAD".

As initial data, the concentrated loads from the wheels of a three-axle car Ni, the coordinates of the points of forces  $x$  of the application of loads, the radius of the arch of the backfill bridge  $R$ , the width of the arch along the ground  $B$  were used.

The vertical pressure from the filling ground and the own weight of the structure are not taken into account, since during field tests it was the relative displacements of the sections from the static test load that were measured.

## 3 BUILDING A GEOMETRIC SCHEME

As a design scheme, a two-hinged, once statically indeterminate circular arch with a radius along the neutral axis  $R = 6$  m, the width of the arch along the edge of the filling  $B = 14$  m, the total width of the arch  $b = 16$  m was adopted. When constructing a geometric scheme, the curved elements of the arch between the nodes located on the axis were replaced by rectilinear rods due to the specifics of constructing flat calculation schemes in the Lira PC.

The step of the arrangement of nodes with numbers  $i = 1,3-49$  on the  $x$  axis in the geometric scheme is 0.5 m. Then each of the 24 circular segments obtained was divided in half by the bisector, and the intersection points of the bisector and the neutral axis were modeled by nodes numbered  $i=2,4-48$ . Number of nodes – 49 pcs. Number of rods -48 pcs.

The load from a three-axle VOLVO FM 400 car with a total weight of 41 tons with a load on the rear trolley of 312 kN and the front axle of 90 kN will be

taken as six concentrated forces (from each wheel in three axes)  $N_{1,2} = 78$  kH;  $N_{3,4} = 78$  kH;  $N_{5,6} = 45$  kH and positioned symmetrically relative to the axis of the roadway with coordinates  $y = \pm 1,05$  m, and relative to the arch lock - according to the loading schemes shown in Figures 1, 2, 3. Loading schemes in Figure 1 correspond to loading schemes when measuring deflections in sections  $n=II, III, IV$  (Safronov, 2010).

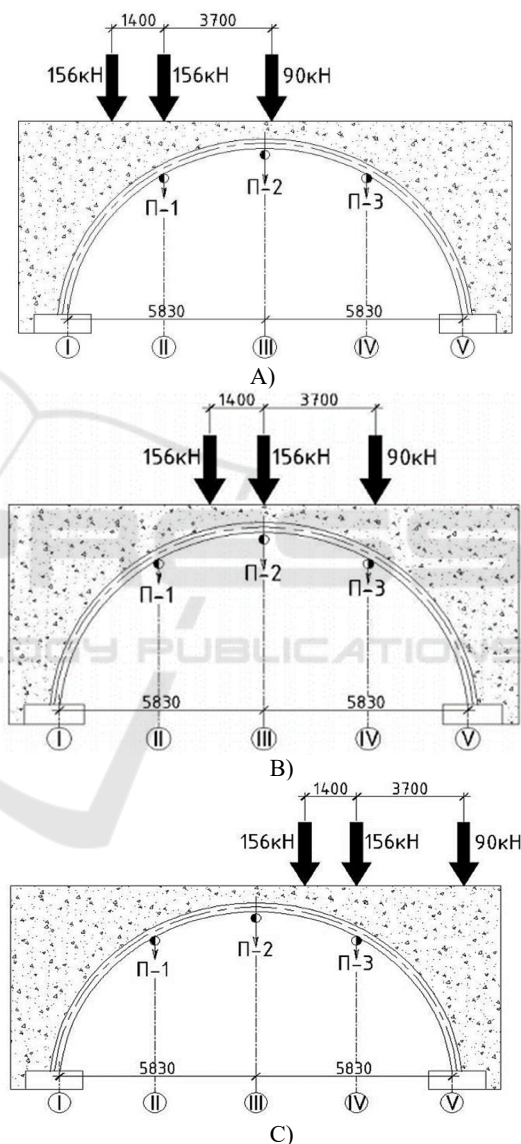


Figure 1: Schemes of loading the bridge with a test load when measuring deflections in the section a)  $n = II$  (Safronov, 2010); b)  $n= III$  (Safronov, 2010); c)  $n=IV$

#### 4 DETERMINATION OF VERTICAL PRESSURE ON THE ARCH SURFACE

The law of distribution and transmission of vertical pressure in a soil mass along the length of the arch span is generally accepted in the form of the Boussinesq problem (Khan, 1998):

$$p_{jnz} = \frac{3 \cdot N_j \cdot z^3}{2 \cdot \pi \cdot (z^2 + x^2 + y^2)^{2.5}} \quad (1)$$

where  $p_{jnz}$  is the value of the transmitted vertical pressure from the force  $N_j$  at the point of the half-space in the section  $n$ ,  $\text{kN/m}^2$  ( $n=II, III, IV$ );

$N_j$  is the value of the concentrated load from the wheel,  $\text{kN}$  ( $j=1, 2, 3, 4, 5, 6$ );

$z$  is the depth of the point at which the pressure is determined;

$x$  is the coordinate of the horizontal projection of the point at which the pressure is determined, relative to the arch lock.

The laws of vertical pressure change  $p_{nz}(x, y)$  have the following form, shown in Figures 2, 3, 4

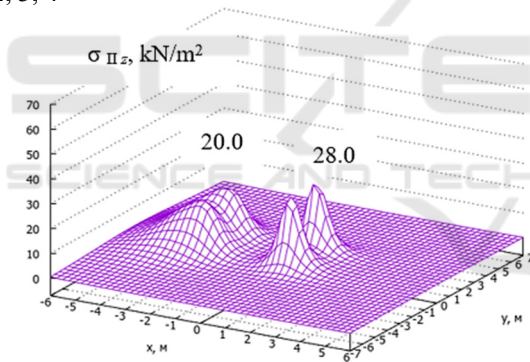


Figure 2: Stress distribution  $p_{II z}$  on the surface of the arch.

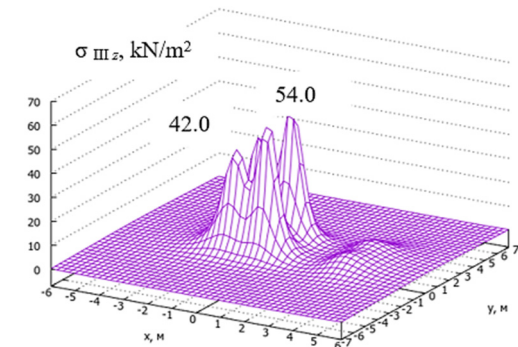


Figure 3: Stress distribution  $p_{III z}$  on the surface of the arch.

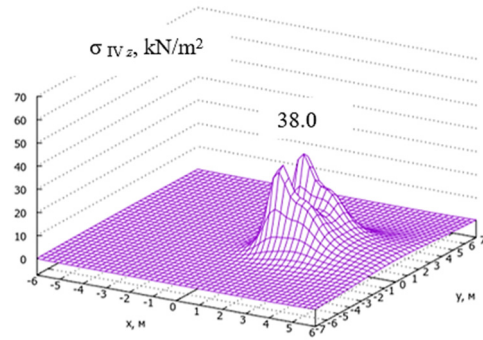


Figure 4: Stress distribution  $p_{IV z}$  on the surface of the arch.

Laws of change of vertical distributed force  $P_{j II z}, P_{j III z}, P_{j IV z}$  ( $\text{kN/m}$ ), allowing to determine the load at any point located on the axis of the arch, from each of the concentrated forces  $N_j$  have the form.

$$P_{1,2 II z}(x) = \int_{-7}^7 117 \frac{((36 - x^2)^{0.5} - 6.67)^3}{\pi \cdot (((36 - x^2)^{0.5} - 6.67)^2 + (x + 4.4)^2 + (y \pm 1.05)^2)^{2.5}} dy \quad (2)$$

$$P_{3,4 II z}(x) = \int_{-7}^7 117 \frac{((36 - x^2)^{0.5} - 6.67)^3}{\pi \cdot (((36 - x^2)^{0.5} - 6.67)^2 + (x + 3)^2 + (y \pm 1.05)^2)^{2.5}} dy \quad (3)$$

$$P_{5,6 II z}(x) = \int_{-7}^7 67,5 \frac{((36 - x^2)^{0.5} - 6.67)^3}{\pi \cdot (((36 - x^2)^{0.5} - 6.67)^2 + (x - 0.7)^2 + (y \pm 1.05)^2)^{2.5}} dy \quad (4)$$

$$P_{1,2 III z}(x) = \int_{-7}^7 117 \frac{((36 - x^2)^{0.5} - 6.67)^3}{\pi \cdot (((36 - x^2)^{0.5} - 6.67)^2 + (x + 1.4)^2 + (y \pm 1.05)^2)^{2.5}} dy \quad (5)$$

$$P_{3,4 III z}(x) = \int_{-7}^7 117 \cdot \frac{((36 - x^2)^{0.5} - 6.67)^3}{\pi \cdot (((36 - x^2)^{0.5} - 6.67)^2 + x^2 + (y \pm 1.05)^2)^{2.5}} dy \quad (6)$$

$$P_{5,6 III z}(x) = \int_{-7}^7 67,5 \frac{((36 - x^2)^{0.5} - 6.67)^3}{\pi \cdot (((36 - x^2)^{0.5} - 6.67)^2 + (x - 3.7)^2 + (y \pm 1.05)^2)^{2.5}} dy \quad (7)$$

$$P_{1,2IVz}(x) = \int_{-7}^{234} \frac{((36 - x^2)^{0.5} - 6.67)^3}{\pi \cdot (((36 - x^2)^{0.5} - 6.67)^2 + (x - 1.6)^2 + (y \pm 1,05)^2)^{2.5}} dy \quad (8)$$

$$P_{3,4IVz}(x) = \int_{-7}^{234} \frac{((36 - x^2)^{0.5} - 6.67)^3}{\pi \cdot (((36 - x^2)^{0.5} - 6.67)^2 + (x - 3)^2 + (y \pm 1,05)^2)^{2.5}} dy \quad (9)$$

$$P_{5,6IVz}(x) = \int_{-7}^{135} \frac{((36 - x^2)^{0.5} - 6.67)^3}{\pi \cdot (((36 - x^2)^{0.5} - 6.67)^2 + (x - 6.7)^2 + (y \pm 1,05)^2)^{2.5}} dy \quad (10)$$

The laws of pressure change are compiled taking into account the minimum filling thickness along the road axis of 0.67 m (Safronov, 2010).

The area of determination of the laws (2) — (10) along the  $x$  axis are the intervals selected taking into account the possibility of transferring pressure from a concentrated force. The boundaries of the intervals are the points of contact with the surface of the arch of radius vectors originating at the place of application of loads  $N_j$  (Figures 5, 6, 7).

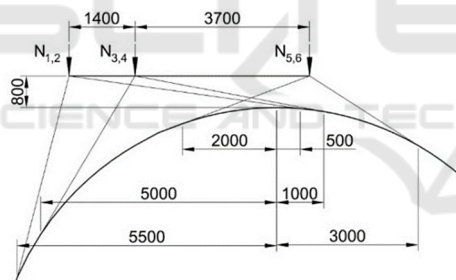


Figure 5: Places where the radius vectors touch the arch surface. Section n=II.

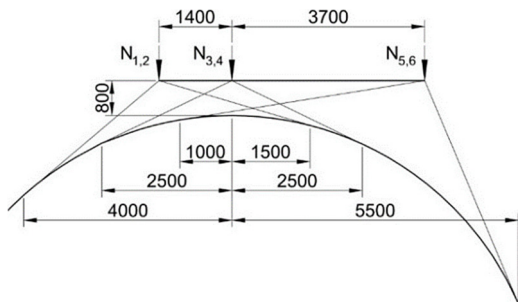


Figure 6: Places where the radius vectors touch the arch surface. Section n=III.

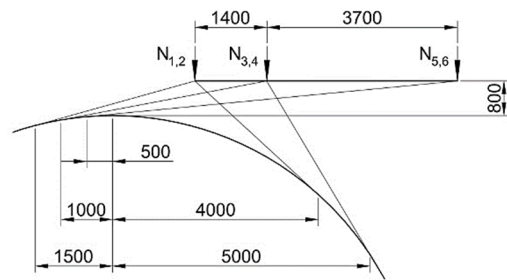


Figure 7: Places where the radius vectors touch the arch surface. Section n=III.

The total ordinates of pressure  $P_{nz}$  over the entire span of the arch for each of the sections  $n$  are found by the superposition principle

$$P_{nz} = \sum_{j=1}^6 P_{jnz} \quad (11)$$

The laws of load change  $P_{nz}(x)$  have the following form, presented in Figures 8, 9, 10.

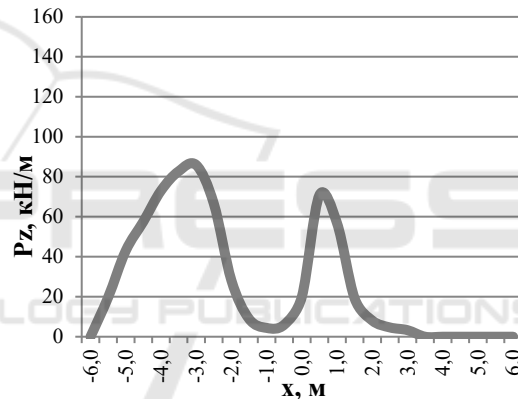


Figure 8: Distributed load values  $P_{IIz}$  along the longitudinal axis of the arch.

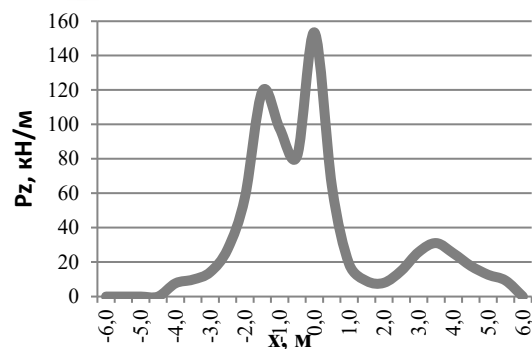


Figure 9: Distributed load values  $P_{IIIz}$  along the longitudinal axis of the arch.

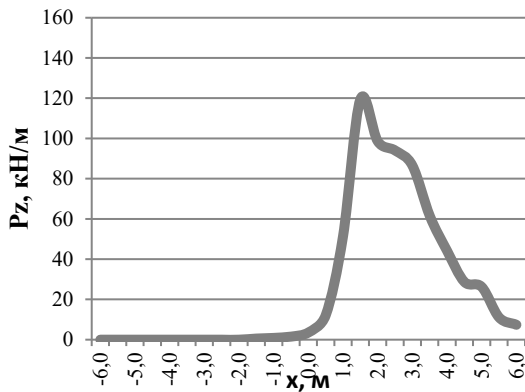


Figure 10: Distributed load values  $P_{IVz}$  along the longitudinal axis of the arch.

### 5 DETERMINATION OF HORIZONTAL PRESSURE ON THE ARCH SURFACE

The law of distribution and transmission of vertical pressure in a soil mass along the length of the arch span is generally accepted in the form of the Boussinesq problem (Khan, 1998):

$$p_{jnx} = \frac{3 \cdot N_j \cdot z^2 \cdot x}{2 \cdot \pi \cdot (z^2 + x^2 + y^2)^{2.5}}, \quad (11)$$

notation in formula (11) – see notation in formula (1).

The laws of change of horizontal pressure  $P_{jnx}$  from each of the concentrated forces along the span length have the form

$$P_{1,2III}(x) = \int_{-7}^{117} \frac{((36 - x^2)^{0.5} - 6.67)^2 \cdot (x + 4.4)}{\pi \cdot (((36 - x^2)^{0.5} - 6.67)^2 + (x + 4.4)^2 + (y \pm 1.05)^2)^{2.5}} dy \quad (12)$$

$$P_{3,4III}(x) = \int_{-7}^{117} \frac{((36 - x^2)^{0.5} - 6.67)^2 \cdot (x + 3.0)}{\pi \cdot (((36 - x^2)^{0.5} - 6.67)^2 + (x + 3.0)^2 + (y \pm 1.05)^2)^{2.5}} dy \quad (13)$$

$$P_{5,6III}(x) = \int_{-7}^{67.5} \frac{((36 - x^2)^{0.5} - 6.67)^3 \cdot (x - 0.7)}{\pi \cdot (((36 - x^2)^{0.5} - 6.67)^2 + (x - 0.7)^2 + (y \pm 1.05)^2)^{2.5}} dy \quad (14)$$

$$P_{1,2IV}(x) = \int_{-7}^{117} \frac{((36 - x^2)^{0.5} - 6.67)^2 \cdot (x + 1.4)}{\pi \cdot (((36 - x^2)^{0.5} - 6.67)^2 + (x + 1.4)^2 + (y \pm 1.05)^2)^{2.5}} dy \quad (15)$$

$$P_{3,4IV}(x) = \int_{-7}^{117} \frac{((36 - x^2)^{0.5} - 6.67)^2 \cdot x}{\pi \cdot (((36 - x^2)^{0.5} - 6.67)^2 + x^2 + (y \pm 1.05)^2)^{2.5}} dy \quad (16)$$

$$P_{5,6IV}(x) = \int_{-7}^{67.5} \frac{((36 - x^2)^{0.5} - 6.67)^3 \cdot (x - 3.7)}{\pi \cdot (((36 - x^2)^{0.5} - 6.67)^2 + (x - 3.7)^2 + (y \pm 1.05)^2)^{2.5}} dy \quad (17)$$

$$P_{1,2IV}(x) = \int_{-7}^{117} \frac{((36 - x^2)^{0.5} - 6.67)^2 \cdot (x - 1.6)}{\pi \cdot (((36 - x^2)^{0.5} - 6.67)^2 + (x - 1.6)^2 + (y \pm 1.05)^2)^{2.5}} dy \quad (18)$$

$$P_{3,4IV}(x) = \int_{-7}^{117} \frac{((36 - x^2)^{0.5} - 6.67)^2 \cdot (x - 3.0)}{\pi \cdot (((36 - x^2)^{0.5} - 6.67)^2 + (x - 3.0)^2 + (y \pm 1.05)^2)^{2.5}} dy \quad (19)$$

$$P_{5,6IV}(x) = \int_{-7}^{67.5} \frac{((36 - x^2)^{0.5} - 6.67)^3 \cdot (x - 6.7)}{\pi \cdot (((36 - x^2)^{0.5} - 6.67)^2 + (x - 6.7)^2 + (y \pm 1.05)^2)^{2.5}} dy \quad (20)$$

The area of determination of the laws (12) — (20) along the  $x$  axis are the intervals selected taking into account the possibility of transferring pressure from a concentrated force (see Figures 7, 8, 9).

The total pressure ordinates  $P_{nx}$  over the entire span of the arch for each of the sections  $n$  are found by the superposition principle

$$P_{nx} = \sum_j^{j=6} P_{jnx}. \quad (21)$$

It is worth noting that the rods with node numbers 1-25 are assigned only those loads  $P_{nx}$  that have a positive direction relative to the  $x$  axis, that is, with a positive sign before the ordinates. Rods with node numbers 25-49 are assigned only those loads  $P_{nx}$  that have a negative direction relative to the  $x$  axis, that is, with a negative sign before the ordinates.

Table 2: Ordinate values of distributed loads.

x, m	i	P II z, kN/m	P III z, kN/m	P IV z, kN/m	P II x, kN/m	P III x, kN/m	P IV x, kN/m
-6.0	1	-	-	-	-	-	-
-5.5	3	19.67	-	-	-5.06	-	-
-5.0	5	43.02	-	-	-14.25	-	-
-4.5	7	57.59	-	-	-13.13	-	-
-4.0	9	73.02	7.72	-	-6.36	-9.13	-
-3.5	11	82.75	9.79	-	4.42	-11.44	-
-3.0	13	85.90	14.15	-	17.64	-15.36	-
-2.5	15	66.60	27.63	-	35.30	-28.42	-
-2.0	17	28.21	57.78	-	27.81	-39.85	-
-1.5	19	8.98	119.41	0.58	11.85	-25.37	-2.10
-1.0	21	4.36	97.55	0.94	2.05	19.33	-3.51
-0.5	23	5.99	81.72	1.57	-5.59	-19.41	-5.22
0.0	25	19.95	153.44	3.64	-18.46	10.28	-9.42
0.5	27	70.85	64.02	12.23	-19.07	49.43	-21.01
1.0	29	56.79	18.75	51.42	23.34	24.89	-44.84
1.5	31	19.15	8.99	119.45	17.81	11.85	-25.64
2.0	33	8.07	7.95	98.59	10.35	1.54	3.66
2.5	35	4.61	15.03	94.06	6.83	-5.82	-0.30
3.0	37	3.27	25.85	86.60	5.10	-12.28	15.86
3.5	39	-	31.06	61.54	-	-3.46	22.97
4.0	41	-	25.03	44.18	-	3.42	19.16
4.5	43	-	17.77	28.74	-	5.26	5.65
5.0	45	-	12.65	26.25	-	4.90	4.00
5.5	47	-	9.25	11.08	-	3.90	-3.11
6.0	49	-	-	7.46	-	-	-0.78

Ordinate values of distributed loads  $P_{IIz}, P_{IIIz}, P_{IVz}, P_{IIx}, P_{IIIx}, P_{IVx}$  are shown in table 2.

3. The values of the coefficients of subgrade reaction for the right half of the arch are similar to those given.

## 6 DETERMINATION OF COEFFICIENTS OF SUBGRADE REACTION

The coefficients of subgrade reaction  $c_1$  for each rod are calculated in accordance with Appendix B (SP 24.13330.2011). The coefficient of subgrade reaction in the Lira PC acts in the direction of the local axis of the rod  $z$ . The calculated value of the coefficient of subgrade reaction is found by the formula

$$c_z = c_1 / \sin \varepsilon, \quad (22)$$

The coefficient of subgrade reaction is set only to those rods whose movement occurs "beyond" the contour of the undeformed circuit.

The values of the coefficients of subgrade reaction for the left half of the arch are given in Table

## 7 DETERMINATION OF DISPLACEMENTS

To determine the displacements of the desired sections  $z_k$ , the authors proposed to use the Mohr method using the rule of A.K. Vereshchagin (Volkov, 2019; Polyakov, 2011).

The displacements were calculated taking into account the influence of longitudinal forces and shearing forces arising in the rods according to the formulas (Polyakov, 2011):

$$Z_{nk} = \sum \int \frac{M_{nz} M_{kz}}{EI_{red}} dx + \sum \int \frac{N_{nz} N_{kz}}{EA_{red}} dx + \sum \int \frac{Q_{nz} Q_{kz}}{GA_{red}} dx,$$

$$X_{nk} = \sum \int \frac{M_{nz} M_{kx}}{EI_{red}} dx + \sum \int \frac{N_{nz} N_{kx}}{EA_{red}} dx + \sum \int \frac{Q_{nz} Q_{kx}}{GA_{red}} dx,$$

Table 3: Calculation of coefficients of subgrade reaction.

i	The depth of the center of gravity of the rod, m	Proportionality coefficient, kN/m <sup>4</sup>	Coefficient of subgrade reaction $c_1$ , kN/m <sup>3</sup>	$\alpha$	Coefficient of subgrade reaction $c_2$ , kN/m <sup>3</sup>
24 25	0.67	6,000	4020	0.017	230341
23 24	0.68		4080	0.070	58489
22 23	0.7		4,200	0.105	40180
21 22	0.74		4440	.139	31903
20 21	0.78		4680	0.191	24527
19 20	0.83		4980	0.225	22138
18 19	0.9		5,400	0.276	19591
17 18	0.97		5820	0.309	18834
16 17	1.06		6360	0.358	17747
15 16	1.16		6960	0.342	20350
14 15	1.27		7620	0.485	15718
13 14	1.41		8460	0.485	17450
12 13	1.55		9300	0.515	18057
11 12	1.71		10260	0.559	18348
10 11	1.9		11400	0.602	18943
9 10	2.09		12540	0.643	19509
8 9	2.32		13920	0.695	20039
7 8	2.57		15420	0.731	21084
6 7	2.86		17160	0.777	22081
5 6	3.19		19140	0.805	23780
4 5	3.58		21480	0.865	24821
3 4	4.04		24240	0.904	26819
2 3	4.86		29160	0.951	30655
1 2	6.06		36360	0.992	36658

where  $M_{nz}$ ,  $Q_{nz}$ ,  $N_{nz}$  are diagrams of bending moments, longitudinal forces and shearing forces from the action of the test load in sections  $n$ ;

$M_{kz}$ ,  $Q_{kz}$ ,  $N_{kz}$  – diagrams of bending moments, longitudinal forces and shearing forces from the action of a single load in the direction of the  $z$  axis at node  $k$ ;

$M_{kx}$ ,  $Q_{kx}$ ,  $N_{kx}$  – diagrams of bending moments, longitudinal forces and shearing forces from the action of a single load in the direction of the  $x$  axis at node  $k$ ;

$E$  – modulus of elasticity of the construction material;

$G$  is the shear modulus of the construction material;

$I_{red}$  is the axial moment of inertia of the reduced section;

$A_{red}$  is the area of the reduced section.

It is advisable to compare with the results of field tests the displacements from the Lira PC, calculated by the formula

$$\Delta_{nk} = \sqrt{X_{nk}^2 + Z_{nk}^2},$$

where  $X_{nk}$  is the horizontal displacement of the  $k$ -th characteristic section of the arch;

$Z_{nk}$  – vertical displacement of the  $k$ -th characteristic section of the arch;

$\Delta_{nk}$  is the total displacement of the  $k$ -th characteristic section of the arch.

Displacements  $X_{nk}$  and  $Z_{nk}$  The complete displacements of the characteristic cross sections of the arch  $\Delta_{nk}$ , mm, located in  $0.25L$ ,  $0.5L$  and  $0.75L$  span are shown in Table 4.

Table 4: Calculated displacements of characteristic sections.

k	$x_k$ , m	$\Delta_{IIk}$ , mm	$\Delta_{IIIk}$ , mm	$\Delta_{IVk}$ , mm
1	-3	-0.16	-0.13	0.14
2	0	-0.14	-0.36	-0.17
3	3	0.10	-0.12	-0.22

Table 5: Comparison of calculation results.

Displacements in calculated sections,		Calculated cross sections, $k$		
		1	2	3
measured during field tests $z_{ne}$ , mm	$z_{IIe}$ , mm	-0.33	-0.10	0.08
	$z_{IIIe}$ , mm	-0.12	-0.41	-0.06
	$z_{IVe}$ , mm	0.10	-0.20	-0.30
calculated in the article (Volkov, 2019) $z_{nk}$ , mm	$z_{IIk}$ , mm	—	—	—
	$z_{IIIk}$ , mm	-0.14	-0.78	-0.36
	$z_{IVk}$ , mm	—	—	—
calculated by the improved method in this paper $\Delta_{nk}$ , mm	$\Delta_{IIk}$ , mm	-0.16	-0.14	0.10
	$\Delta_{IIIk}$ , mm	-0.13	-0.36	-0.12
	$\Delta_{IVk}$ , mm	0.14	-0.17	-0.22

## 8 COMPARISON OF THE OBTAINED RESULTS WITH THE RESULTS OF A FULL-SCALE EXPERIMENT

For the convenience of comparing the existing results with the results obtained, we will summarize them in Table 5.

## 9 CONCLUSIONS

We hope you find the information in this template useful in the preparation of your submission.

Comparing the calculated values of  $\Delta k$  with the calculated values obtained by modeling the structure in the Lira PC zk, as well as with the displacements obtained during full-scale tests of ze, it can be noted that the values calculated according to the method proposed by the authors have deviations of up to 17 percent from the values obtained during full-scale tests. It is also worth noting that the deviations of the results obtained during the study are 5 times less than the deviations obtained during the calculation in (Volkov, 2019) when compared with the results of field tests.

Thus, the computational model using the theory of a linearly deformable half-space proposed by the authors for calculating the pressure acting from temporary loads reliably reflects the work of backfill structures, which allows us to apply the problems of elasticity theory with a sufficient degree of accuracy to describe the distribution of stresses in the soil from temporary loads when collecting loads on the load-bearing elements of backfill bridges.

## REFERENCES

- Safronov, V. S., Zazvonov, V. V., 2010. Full-scale static tests of a backfill road bridge with a vaulted span made of monolithic reinforced concrete. *Construction mechanics and structures*, No. 1., pp. 29-38.
- Volkov, N. V., Permikin, A. S., 2019. Analytical calculation of a backfill bridge. *Perspective*, No. 2., pp. 4-18.
- Khan, H., 1988. *Theory of Elasticity: Fundamentals of linear theory and its application: textbook*. Mir, 344 p.
- SP 24.13330.2011 with amendments No. 1, 2, 3. *Pile foundations: set of rules: official publication: approved and put into effect by Order of the Ministry of Regional Development of the Russian Federation (Ministry of Regional Development of Russia) dated December 27, 2010 N 786: updated version of SNiP 2.02.03-85: date of introduction 20-05-2011. Developed by N.M. Gersevanov Research Institute – Institute of JSC "Research Center "Construction", 2019. Standartinform.*
- Polyakov, A. A., Koltsov, V. M., 2011. *The resistance of materials and the fundamentals of the theory of elasticity: textbook 2nd ed. revised and corrected*. UrFU, 527 p.
- Rubin, O. D., Lisichkin, S. E., Shestopalov, P. V., 2016. Features of mathematical finite element modeling of systems "concrete structure under construction - non-rock foundation". *In construction mechanics of engineering structures and buildings*. No. 2., pp. 63-67.
- Gorbunov-Posadov, M. I., Ilyichev, V. A., Krutov, V. I., 1985. *Bases, foundations and underground structures: designer's handbook*. Stroyizdat, 480 p.
- Shamshina, K. V., Migunov, V. N., Ovchinnikov, I. G., 2018. *IOP Conf. Ser.: Mater. Sci. Eng.* 451, 012058.
- Permikin, A. S., Ovchinnikov, I. G., and Gricuk, A. I., 2020. *Russian Journal of Transport Engineering* 4.
- Spangler, M. G., 1960. *Soil engineering 2nd ed.* Scranton: International textbook company.



- Heger, F. J., *Transportation Research Board 878*, 1982.  
pp. 93-100.
- Heger, F. J., Liepins, A. A., Selig, E. T., 1985.  
*Transportation Research Board 1008*.
- Kevin, L. A., 2016. *A review of depth of cover tables for  
concrete and corrugated metal pipe for the Iowa  
Department of Transportation*.
- Erdogmus, E., Skourup, B. N., Tadros, M., 2010. *Journal  
of pipeline systems and practice 1*, pp. 25-32.

